Journal of Nonlinear Modeling and Analysis
Volume 8, Number 1, February 2026, 170–184
https://global-sci.com/jnma
DOI:10.12150/jnma.2026.170

Nonlinear Dynamics and Pull-in Phenomena in a Magneto-Electro MEMS Actuator with Hardening Spring*

Lijun Zhang[1,2†] and Jun Ma[3]

Received 13 April 2025; Accepted 16 June 2025

Abstract This paper investigates the dynamic behavior and pull-in instability of a magneto-electro Micro-Electro-Mechanical System (MEMS) actuator, focusing on the nonlinear effects arising from magnetic forces and spring stiffness. The system consists of a movable wire attracted toward a stationary wire due to magnetic forces generated by applied currents. A critical equilibrium, known as the pull-in point, is reached when the currents exceed a threshold, leading to instability. We consider the governing equation based on Newton's Second Law, incorporating a nonlinear restoring force for the spring, which exhibits hardening behavior. The resulting second-order differential equation is analyzed using qualitative and bifurcation theories, revealing the critical bifurcation values determined by the currents and spring stiffness. Through a dynamical systems approach, we characterize the phase portraits and solutions, identifying distinct dynamical behaviors and the conditions for pull-in instability. Numerical simulations are performed to validate the analytical predictions, demonstrating excellent agreement with the theoretically derived threshold.

Keywords MEMS, magneto-electro actuator, nonlinear hardening spring, pull-in instability, bifurcation and qualitative analysis

MSC(2010) 34C23, 37G15, 74H45, 74F15.

1. Introduction

Micro-Electro-Mechanical Systems (MEMS) are highly integrated devices that combine electrical, mechanical, and sensing components at the micro- or nano-scale, with typical dimensions and motion ranges measured in micrometers. As a key

†the corresponding author.
Email address:li-jun0608@163.com (L. Zhang)
[1]School of Science, Zhejiang University of Science and Technology, Liuhe Road, 310023 Hangzhou, China
[2]Material Science, Innovation and Modelling Research Focus Area, North-West University, Mafikeng Campus, 2735 Mmabatho, South Africa
[3]College of Mathematics and Systems Science, Shandong University of Science and Technology, 266590 Qingdao, China
*This work is supported by National Natural Science Foundation of China (12172199).

technology in modern micro- and nano-engineering, MEMS achieve miniaturization, high integration, and intelligent functionality. Unlike traditional mechanical engineering, MEMS fabrication relies on advanced semiconductor processes, such as photolithography, etching, and thin-film deposition, ensuring compatibility with integrated circuits and leveraging micro- and nano-fabrication techniques [1]. This approach enables MEMS to realize complex mechanical structures with high precision, reliability, and low power consumption.

Recent advancements in fabrication technologies have significantly expanded the capabilities of MEMS, enabling the development of novel microstructures such as micro-sensors, micro-actuators, and micro-resonators [2]. These innovations have enhanced MEMS performance in terms of accuracy, reliability, and adaptability, opening new application possibilities in biomedical engineering, aerospace, consumer electronics, and industrial automation [3, 4]. However, the dynamic behavior of MEMS devices often exhibits strong nonlinearities, such as nonlinear elastic forces, electrostatic coupling, and micro-scale damping effects [5, 6]. These nonlinear characteristics pose significant challenges to the dynamic response, stability, and control of MEMS. A thorough investigation into the dynamic properties of MEMS, including the mechanisms of nonlinear behavior and effective control strategies, is essential for optimizing performance and expanding application potential [7, 8].

The MEMS device under consideration consists of a stationary wire connected to a voltage source and a movable wire. When a voltage is applied, the movable wire is attracted toward the stationary one due to the magnetic force generated by the current. A critical equilibrium, known as the pull-in point, is reached when the currents in both wires exceed a threshold value. Beyond this threshold, if the current increases further, the movable wire will come into contact with the stationary wire, causing the microstructure to deviate from its optimal position. This phenomenon is referred to as pull-in instability, a significant nonlinear behavior in MEMS where the moving part approaches the actuating electrode. It is influenced by various parameters of the forces involved in the actuation and manipulation within the MEMS device [9, 10]. Nayfeh et al. [11] investigated pull-in instability in MEMS resonators, highlighting the distinct effects of Alternating Current (AC) and Direct Current (DC) loads. Their research, which focused on dynamic pull-in, provided essential guidelines for the safe design of MEMS resonant sensors. Zhang et al. [12] conducted a comprehensive review of the pull-in phenomenon in electrostatic MEMS and NEMS, elucidating the underlying physical principles responsible for instability and device failures. They also summarized the governing equations and conditions for predicting various pull-in behaviors. In recent years, the pull-in phenomenon in MEMS has garnered significant attention from researchers, who have employed diverse methodologies to explore its mechanisms and implications.

According to Newton's Second Law of Motion, the dynamics of a typical magneto-electro MEMS actuator can be described by the governing equation:

$$m\frac{d^2u}{dT^2} + F_s = F_e. \tag{1.1}$$

Here m is the mass of the movable current-carrying wire, u is the deformation length of the spring, F_s is the restoring force of the spring, and F_e represents the magnetic attraction force between the conductors.

The magnetic attraction force between the conductors due to the magnetic fields

produced by the currents i_1 and i_2 is given by

$$F_e = \frac{\mu_0 i_1 i_2 l}{2\pi(b-u)}, \tag{1.2}$$

where $\mu_0 = 4\pi \times 10^{-7} N/A^2$ is the magnetic coefficient, i_1 and i_2 are the electronic currents in the adjacent wires, l is the wire's length, b is the distance between the two wires when the spring has no deformation [13] (see Fig. 1).

As for the restoring force of the spring F_s, the simplest model equation is the linear equation described by Hooke's Law, that is, it is proportional to the displacement from the equilibrium position, written as $F_s = k_1 u$. He et al. [14] examined the dynamic pull-in of conductor-magnetoelectric devices modeled by (1.1) with a linear restoring force of the spring, and derived a threshold for instability based on model parameter assessments. Skrzypacz et al. [15] proposed a model for a magnetic Micro-Electro-Mechanical Structure actuator with linear spring and current carrying filaments, analyzed the pull-in dynamics and presented the approximate periodic solutions. Wang et al. [16] studied the pull-in instability in MEMS with linear spring and a conductor actuated at a free position and identified the existence of the unique threshold for system stability. Liu et al. [17] analyzed pull-in instability in electrostatic MEMS actuators accounting for edge effects by using the dynamic system method and qualitative analysis of differential equations. i The existence and bifurcations of the periodic solution of the model equation for an electrostatically actuated MEMS system's mass-spring model with damping force is investigated in [18] by using the continuation theorem, along with a priori estimates and bifurcation theory. Their work revealed that the system exhibits various dynamic behaviors, including saddle-node and period-doubling bifurcations.

In real-world systems, the linear restoring force, described by Hooke's Law, is only valid for small displacements. For larger displacements, nonlinear effects become significant, and the restoring force can be modeled as:

$$F_s = k_1 u + k_3 u^3, \tag{1.3}$$

where $k_1 > 0$ is the linear stiffness coefficient and k_3 is the nonlinear stiffness coefficient for the spring. It is a linear spring when $k_3 = 0$. A positive k_3 indicates that the spring exhibits hardening nonlinearity and a negative k_3 indicates that the spring exhibits softening nonlinearity. Then the model equation (1.1) can be explicitly written as

$$m\frac{d^2u}{dT^2} + k_1 u + k_3 u^3 - \frac{\mu_0 i_1 i_2 l}{2\pi(b-u)} = 0, \tag{1.4}$$

which is a second-order differential equation with singularity at $u = b$. This model equation has been considered in [19] and a threshold for pull-in instability is derived. Unfortunately, the threshold is tested to be incorrect numerically (refer to the numerical simulations in Section 3).

In this work, we consider the MEMS with the spring exhibits hardening nonlinearity, that is, we focus on equation (1.1) with $k_3 > 0$. Qualitative and bifurcation theories are powerful tools for analyzing parameterized second-order differential equations and have been widely applied in the study of various nonlinear differential systems [20–22]. In this work, we rewrite the non-dimensional governing equation as a planar dynamical system and employ the dynamical systems approach to analyze the bifurcation value and phase portraits. Through mathematical analysis, we

reveal the existence of a critical bifurcation value determined by the currents i_1 and i_2, which varies with the stiffness of spring in the MEMS.

The paper is organized as follows. In Section 2, we normalize the governing equation to a nonlinear ordinary differential equation (ODE) with two parameters and a singularity. Using a dynamical systems approach, we analyze the bifurcation and phase portraits in each bifurcation set, characterizing solutions that exhibit distinct dynamical behaviors. Section 3 investigates the pull-in instability of the MEMS actuator from a physical perspective, providing insights into the underlying mechanisms. Finally, concluding remarks are presented in the last section.

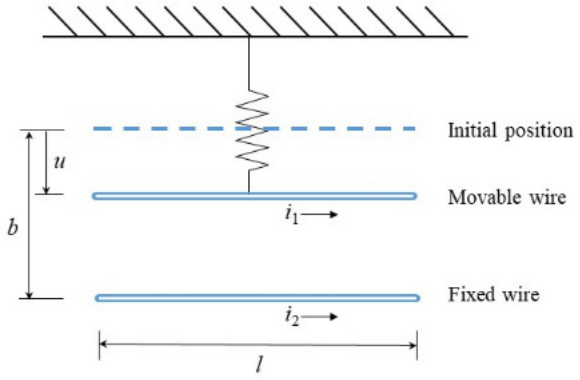

Figure 1. Schematic of a single-degree-of-freedom spring-mass system with parallel-wire configuration

2. Dynamical analysis of the model equation

For convenience and simplification the model equation (1.4), we introduce the new parameters $k = \frac{k_3}{k_1}b^2$, $w_0^2 = \frac{k_1}{m}$, $I = \frac{\mu_0 i_1 i_2 l}{2\pi k b^2}$, and the following transformations $x = \frac{u}{b}$, $t = Tw_0$, to obtain an equivalent equation

$$\frac{d^2x}{dt^2} + x + kx^3 = \frac{I}{1-x}. \tag{2.1}$$

By setting $\dot{x} = y$, we rewrite equation (2.1) as the following system

$$\frac{dx}{dt} = y, \quad \frac{dy}{dt} = \frac{I}{1-x} - x - kx^3, \tag{2.2}$$

which is a Hamiltonian system with the Hamiltonian

$$H(x,y) = \frac{1}{2}y^2 + \frac{1}{2}x^2 + \frac{1}{4}kx^4 + I\ln|1-x|. \tag{2.3}$$

To characterize the dynamics of the concerned spring-mass system, one needs to explore the dynamical properties of the solutions of system (2.2). Clearly, this system is a planar dynamical system with singularity on the line $x = 1$. For the case when $1 - x \neq 0$, by the rescaling $dt = (1-x)d\tau$, system (2.2) is transformed to

$$\frac{dx}{d\tau} = y(1-x), \quad \frac{dy}{d\tau} = x(x-1)(kx^2+1) + I. \tag{2.4}$$

Note that system (2.4) shares identical topological phase portraits with system (2.2) with the exception of the singular line $x = 1$. Moreover, in the $xy-$phase plane where $x > 1$, the corresponding trajectories of the two systems (2.2) and (2.4) have the same direction; while in the xy-phase plane where $x < 1$, the corresponding trajectories have opposite direction. Recall that the dependent variable is introduced through the rescaling $x = \frac{u}{b}$. Given that the variable u in the original model equation is physically constrained to $u < b$, it follows that the dimensionless variable x in system (2.4) is physically meaningful only when $x < 1$. Therefore, in the subsequent sections of this paper, we consistently assume that $x < 1$.

Based on the dynamical system theory, one needs to examine the equilibrium points of system (2.4) to acquire its dynamical properties. If setting

$$g(x) = x(x-1)(kx^2+1) + I, \tag{2.5}$$

then we see that the zeros of $g(x)$ define the equilibrium points of system (2.4).

Lemma 2.1. *For $k \geq 0$, there exists a unique $x_1 \in (0,1)$ where the function $g(x)$ attains its minimum. Furthermore, $g(x)$ decreases on $(-\infty, x_1)$ while it increases on $(x_1, 1)$.*

Proof. Differentiating twice successively on equation (2.5) with respect to x yields

$$g'(x) = 4kx^3 - 3kx^2 + 2x - 1 \tag{2.6}$$

and

$$g''(x) = 12kx^2 - 6kx + 2. \tag{2.7}$$

Let us first consider the case when $0 \leq k \leq \frac{8}{3}$. It is easy to see that $g''(x) \geq 0$ and consequently $g'(x)$ increases on the real line in this case. It follows from (2.6) that $g'(1) = k + 1 > 0$ and $g'(0) = -1 < 0$. Hence, $g'(x)$ has a unique zero, which we denote by x_1. Then $0 < x_1 < 1$, $g'(x) < 0$ on $(-\infty, x_1)$ and $g'(x) > 0$ on $(x_1, 1)$. Therefore, the function $g(x)$ decreases on $(-\infty, x_1)$ but increases on $(x_1, 1)$, which indicates that $g(x)$ attains its minimum at $x = x_1$.

We now consider the case when $k > \frac{8}{3}$. Clearly, $g''(x) = 0$ has two roots $x_\pm = \frac{1}{4}\left(1 \pm \sqrt{1 - \frac{8}{3k}}\right)$, where $0 < x_- < x_+ < \frac{1}{2}$. It results in that $g'(x)$ increases on $(-\infty, x_-)$ and (x_+, ∞), while it decreases on (x_-, x_+). Hence, the function $g'(x)$ attains its maximum at $x = x_-$ and minimum $g'(x_+)$ at $x = x_+$. Since

$$g'(x_-) = \frac{1}{2}\left(\frac{8}{3} - k\right)x_- - \frac{5}{6} < 0,$$

one has $g'(x) < 0$ for $x < x_+$. Note that $g'(1) = k + 1 > 0$. Therefore, $g'(x)$ has a unique zero in $(-\infty, 1)$. Denote the unique zero of $g'(x)$ by x_1, namely, $g'(x_1) = 0$, then $g'(x) < 0$ for $x < x_1$ and $g'(x) > 0$ for $x_1 < x < 1$. It follows that $g(x)$ decreases on $(-\infty, x_1)$ while it increases on $(x_1, 1)$. This completes the proof. □

Remark 2.1. It follows directly from the proof above that the critical point x_1 proposed in Lemma 2.1 is the minimum point for function $g(x)$, which is actually determined uniquely by equation (2.6) for the case when $k \geq 0$. Therefore, x_1 varies with k but is independent of I. Although $x_1 \in (0,1)$, its value generally cannot be expressed exactly.

Denote

$$\phi(x) = \frac{1}{16}(3k-8)x^2 + \frac{5}{8}x + \frac{1}{16}.$$

Then, we have

Lemma 2.2. *For $x_1 \in (0,1)$ determined implicitly by equation (2.6), the following properties hold for function $g(x)$ that*

(1) $g(x) > 0$ when $I > \phi(x_1)$;

(2) $g(x) > 0$ for $x \neq x_1$ and $g(x_1) = 0$ when $I = \phi(x_1)$;

(3) it possesses exactly two distinct zeros x_{e_1} and x_{e_2} such that $0 < x_{e_1} < x_1 < x_{e_2} < 1$ when $0 < I < \phi(x_1)$. Moreover, $g(x) > 0$ for $x \in (-\infty, x_{e_1}) \cup (x_{e_2}, 1)$ and $g(x) < 0$ for $x \in (x_{e_1}, x_{e_2})$.

Proof. From equations (2.5) and (2.6), one has

$$g(x_1) = \frac{1}{16}(8-3k)x_1^2 - \frac{5}{8}x_1 - \frac{1}{16} + I.$$

Recall from Lemma 2.1 that $g(x)$ attains its minimum at $x = x_1$. Hence $g(x)$ has no zero if $g(x_1) > 0$; it has a double zero at $x = x_1$ if $g(x_1) = 0$; while it has two zeros if $g(x_1) < 0$. The first two statements follow directly by noting that $g(x_1) > 0$ when $I > \phi(x_1)$ and $g(x_1) = 0$ when $I = \phi(x_1)$.

It is easy to see that $g(0) = g(1) = I > 0$, while $g(x_1) < 0$ when $I < \phi(x_1)$. It follows that $g(x) = 0$ has two roots at x_{e_1} and x_{e_2} such that $0 < x_{e_1} < x_1 < x_{e_2} < 1$ by the intermediate value theorem of continuous functions. This completes the proof. □

Since the equilibrium points of system (2.4) are determined by the zeros of $g(x)$, it follows directly from Lemma 2.2 that system (2.4) has no equilibrium point when $I > \phi(x_1)$; it admits one equilibrium point $(x_1, 0)$ for $x = 1$; while it admits two equilibrium points $(x_{e_1}, 0)$ and $(x_{e_2}, 0)$ for $x < 1$. According to dynamical systems theory [23], the local behavior of system (2.4) near an equilibrium point can be determined by analyzing the eigenvalues of its linearization at this critical point. The Jacobian matrix of the system at an equilibrium point $(x_0, 0)$ is given by

$$A(x_0, 0) = \begin{pmatrix} 0 & 1 - x_0 \\ g'(x_0) & 0 \end{pmatrix}.$$

Considering the trace and determinant of matrix $A(x_0, 0)$, it is found that the trace equals zero and the determinant is given by $-(1-x_0)g'(x_0)$. Therefore, the matrix $A(x_0, 0)$ admits two real eigenvalues with opposite signs when $-(1-x_0)g'(x_0) < 0$; while it has two purely imaginary conjugate eigenvalues when $-(1-x_0)g'(x_0) > 0$. Taking into account the fact that system (2.4) is an integrable planar dynamical system, we see that $(x_0, 0)$ is a saddle for system (2.4) if $-(1-x_0)g'(x_0) < 0$; it is a cusp if $-(1-x_0)g'(x_0) = 0$; while it is a center for system (2.4) if $-(1-x_0)g'(x_0) > 0$.

Lemma 2.3. *For x_1 determined implicitly by $4kx_1^3 - 3kx_1^2 + 2x_1 - 1 = 0$, the following properties hold for system (2.2):*

(1) when $I > \phi(x_1)$, it has no equilibrium point;

(2) when $I = \phi(x_1)$, it possesses a cusp $(x_1, 0)$;

(3) when $I < \phi(x_1)$, it possesses only a center $(x_{e_1}, 0)$ and a saddle $(x_{e_2}, 0)$ such that $0 < x_{e_1} < x_1 < x_{e_2} < 1$.

Proof. The first two statements follow directly from Lemma 2.2 and the dynamical system theory. Similarly, we find that system (2.4) possesses only a saddle $(x_{e_2}, 0)$ and a center $(x_{e_1}, 0)$ such that $0 < x_{e_1} < x_1 < x_{e_2} < 1$ by the observing that $-(1 - x_{e_1})g'(x_{e_1}) > 0$ and $-(1 - x_{e_2})g'(x_{e_2}) < 0$ for $I < \phi(x_1)$. □

When setting $h = H(x_0, y_0)$, the orbit of system (2.2) passing through the point (x_0, y_0) is determined by equation

$$H(x, y) = \frac{1}{2}y^2 + \frac{1}{2}x^2 + \frac{1}{4}kx^4 + I\ln|1 - x| = h, \tag{2.8}$$

equivalently,

$$y^2 = -\frac{1}{2}kx^4 - x^2 - 2I\ln(1 - x) + 2h \tag{2.9}$$

since the study is restricted to $x < 1$ based on physical considerations. Denote

$$h(x) = H(x, 0) = \frac{1}{4}kx^4 + \frac{1}{2}x^2 + I\ln(1 - x).$$

Then it follows that

$$h'(x) = \frac{-x(x - 1)(kx^2 + 1) - I}{1 - x} = \frac{-g(x)}{1 - x},$$

which implies that $h'(x)$ has opposite sign to $g(x)$. Therefore, the function $h(x)$ decreases with x on the interval where $g(x) \geq 0$ and increases on the interval where $g(x) \leq 0$. And equation (2.9) is equivalent to $y^2 = 2(h - h(x))$, which indicates that the trajectory is well-defined on the interval $\{x|h \geq h(x)\}$. It follows directly from Lemma 2.2 that function $h(x)$ decreases on the interval $(-\infty, 1)$ when $I \geq \phi(x_1)$; while it decreases on $\in (-\infty, x_{e_1}) \cup (x_{e_2}, 1)$ and increases on the interval (x_{e_1}, x_{e_2}) when $I < \phi(x_1)$.

Due to the physical constraints of the system, we restrict our analysis to solutions of equation (2.1) with initial conditions $x(0) = x_0 < 1$ and $x'(0) = 0$. Consequently, we only consider the trajectories of system (2.2) that originate from points $(x_0, 0)$ with $x_0 < 1$ which is determined by equation (2.9) with $h = H(x_0, 0)$ such that $h(x) \leq h$.

We next discuss the trajectories of system (2.2) in the following three cases.

(1) When $I > \phi(x_1)$, the function $h(x)$ decreases on the interval $(-\infty, 1)$, and thus $h(x) < h = h(x_0) = H(x_0, 0)$ for arbitrary $x_0 < 1$ and $x_0 \leq x < 1$. It implies that equation (2.9) is well defined on the interval $[x_0, 1)$. Moreover, one can see from equation (2.9) and the monotonicity of the function $h(x)$ that the trajectory is symmetrical with respect to the x-axis, increases in the plane above x-axis and approaches asymptotically the singular line $x = 1$.

(2) When $I = \phi(x_1)$, for arbitrary $x_0 < 1$ with $x_0 \neq x_1$, similarly as the case $I > \phi(x_1)$, we see that the trajectory approaches asymptotically the singular line $x = 1$. However, for $x_0 = x_1$, $x = x_1$ is the solution of equation (2.1). For $h = H(x_1, 0)$, equation (2.9) can be written as

$$y^2 = -\frac{1}{2}kx^4 - x^2 - 2\phi(x_1)\ln(1 - x) + 2H(x_1, 0), \tag{2.10}$$

which is well defined for $x \in (x_1, 1)$ because the function of x in the right-hand side of equation (2.10) is valued 0 at $x = x_1$ and increasing on $(x_1, 1)$. In particular, it

approaches positive infinity as $x \to 1^+$. Therefore, equation (2.10) defines a curve symmetrical to the x-axis for $x \in [x_1, 1)$ and the part above x-axis is an increasing curve which approaches $x = 1$ asymptotically. By the theory of dynamical system, one sees that the curve corresponding to $h = H(x_1, 0)$ is a stable (resp. unstable) manifold at the cusp $(x_1, 0)$ when it is above (resp. below) the x-axis.

(3) When $0 < I < \phi(x_1)$, one has from Lemma 2.3 that system (2.2) admits a saddle $(x_{e_1}, 0)$ and a center $(x_{e_2}, 0)$ with $0 < x_{e_1} < x_1 < x_{e_2} < 1$. It follows directly from equation (2.8) that $H(x, 0) \to \infty$ as $x \to -\infty$ and $H(x, 0) \to -\infty$ as $x \to 1^-$ for $I > 0$. It holds that $H(x_{e_1}, 0) < H(x_{e_2}, 0)$ since $H(x, 0)$ increases on the interval (x_{e_1}, x_{e_2}) when $I < \phi(x_1)$.

To examine the trajectory passing through the saddle $(x_{e_2}, 0)$, one can study equation

$$y^2 = -\frac{1}{2}kx^4 - x^2 - 2I\ln(1-x) + 2H(x_{e_2}, 0) = 2(H(x_{e_2}, 0) - h(x)). \tag{2.11}$$

On can see from the monotonicity of function $h(x)$ that there is $x_l < x_{e_1}$ such that $h(x_{e_2}) = H(x_{e_2}, 0) = H(x_l, 0)$, $h(x) > H(x_l, 0)$ on the interval $(-\infty, x_l)$ and $h(x) \le H(x_l, 0)$ on the interval $(x_l, 1)$, which indicates that equation (2.11) is well defined for $x > x_l$. Thus the corresponding trajectory consists of a closed curve Γ_h passing through two points $(x_l, 0)$ and the saddle $(x_{e_2}, 0)$, and two curves passing through the saddle, among which the one above (resp. below) x-axis S^u (resp. Ss) increases (resp. decreases) and asymptotically approaches the line $x = 1$. By the dynamical system theory, one sees that Γ_h is the so-called homoclinic orbit, W^u is an unstable manifold which tends to $(x_{e_1}, 0)$ as $t \to -\infty$ and W^s is a stable manifold which tends to $(x_{e_1}, 0)$ as $t \to \infty$.

Similarly, since the function $h(x)$ attains its minimum at $x = x_{e_1}$, equation (2.11) is well defined on the interval $[x_l, x_m]$ and $[x_r, 1)$ for $h \in [h(x_{e_1}), h(x_{e_2}))$, where $x_l \le x_m < x_r$ such that $h(x_l) = h(x_m) = h(x_r) = h$. That implies that the corresponding trajectory consists of two separated curves: a closed curve Γ_h passing through two points $(x_l, 0)$ and $(x_{e_m}, 0)$, and another one passing through $(x_r, 0)$ which asymptotically approaches the line $x = 1$. Note that the closed curve Γ_h constricts to a point $(x_{e_1}, 0)$ for $h = h(x_{e_1})$. However, for $h = h(x_0) < h(x_{e_1})$, where $x_0 > x_{e_2}$, equation (2.11) is well defined on the interval $[x_0, 1)$, and it defines a curve asymptotically approaching the line $x = 1$.

We conclude the results above in the following theorem.

Theorem 2.1. *For x_1 determined implicitly by $4kx_1^3 - 3kx_1^2 + 2x_1 - 1 = 0$, the following properties hold for system (2.2):*

(1) when $I > \phi(x_1)$, all orbits asymptotically approach the straight line $x = 1$ (see Fig. 2(a));

(2) when $I = \phi(x_1)$, there is a stable manifold and an unstable manifold at the cusp $(x_1, 0)$. Moreover, all orbits asymptotically approach the singular line $x = 1$ (see Fig. 2(b));

(3) when $0 < I < \phi(x_1)$, there is a family of closed periodic trajectories surrounding the center $(x_{e_2}, 0)$, which is bounded by a homoclinic orbit at the saddle $(x_{e_1}, 0)$. There are another two manifolds in the plane $x > x_{e_1}$, one stable and one unstable. Both of them asymptotically approach the singular line $x = 1$. The stable one tends to $(x_{e_1}, 0)$ as $t \to \infty$, while the unstable one tends to $(x_{e_1}, 0)$ as $t \to -\infty$. All other trajectories asymptotically approach the singular line $x = 1$ (see Fig. 2(c)).

Lemma 2.4. *Along the trajectory of system* (2.2) *which asymptotically approaches the singular line* $x = 1$, $x(t)$ *tends to 1 in a finite time.*

Proof. Since $h(x)$ is strictly decreasing on some left neighborhood of $x = 1$, any trajectory of system (2.2) approaching $x = 1$ above the x-axis must pass through some point (x_1, y_1) such that $h(x)$ decreases on $(x_1, 1)$ and $y_1 > 0$. Since the trajectory above the x-axis is given by $y = \sqrt{2(H(x_1, y_1) - h(x))}$, we have $y(x) > y_1$ for $x \in (x_1, 1)$. From the first equation of system (2.2), it follows that $\frac{dx}{dt} = y \geq y_1$, and thus $x(t) \geq x_1 + y_1(t - t_0)$, where t_0 is the travel time from the initial point to (x_1, y_1) along the trajectory. Taking into account that $x < 1$, we have $t < t_0 + \frac{1-x_1}{y_1}$, that is, it takes finite time for $x(t)$ tending to 1 along the trajectory which approaches the singular line $x = 1$. □

Lemma 2.4 indicates that the solution to equation (2.1) blows up in finite time if the trajectory asymptotically approaches the singular line. It is important to note that equation (2.1), studied in this work, arises in the context of MEMS. For a magneto-electrostatic MEMS actuator, if the device is launched from an initial position x_0 with zero speed, the initial conditions $x(0) = x_0$ and $x'(0) = 0$ must be applied to equation (2.1). Accordingly, the following statements hold for equation (2.1).

Theorem 2.2. *Consider equation* (2.1) *subject to the initial value* $x(0) = x_0, x'(0) = 0$. *Assume* x_1 *is the unique zero of the cubic equation* $4kx^3 - 3kx^2 + 2x - 1 = 0$ *with* $k > 0$.

(1) For $I > \phi(x_1)$, *the solution* $x(t)$ *blows up at* $x = 1$ *in a finite time* t_0. *More precisely, there exists* $t_0 > 0$ *such that* $x(t) \to 1^-$ *as* $t \to t_0^-$;

(2) For $I = \phi(x_1)$, *the solution blows up at* $x = 1$ *in a finite time* t_0 *if* $x_0 \neq x_1$, *while* $x = x_1$ *is an unstable equilibrium state of the equation when* $x_0 = x_1$;

(3) For $0 < I < \phi(x_1)$, *the equation has two equilibrium states: a stable equilibrium at* $x = x_{e_2}$ *and an unstable equilibrium at* $x = x_{e_1}$. *Equation* (2.1) *exhibits the following behaviors:*

- ***Periodic Solutions****: When* $x_0 \in (x_c, x_{e_1}) \cup (x_{e_1}, x_{e_2})$, *where* x_c *is determined by* $h(x_c) = h(x_{e_2})$, *the equation admits a periodic solution.*
- ***Convergent Solutions****: For* $x_0 = x_c$, *the solution increases with time and approaches the stable equilibrium* x_{e_2} *as* $t \to \infty$.
- ***Blow-up Solutions****: For* $x_0 \in (-\infty, x_c) \cup (x_{e_2}, 1)$, *the solution increases and blows up at* $x = 1$ *in finite time.*

3. Pull-in instability in magnetoelectric MEMS actuator

In the micro-electromechanical system considered in this work, the flexible wire moves under the combined action of the electromagnetic force generated by the electric current and the elastic force of the spring, exhibiting inherent strong nonlinearity, which has been revealed by the mathematical analysis results in last section. The flexible wire may exhibit periodic motion, tend toward an unstable equilibrium state, or experience a sudden collapse, rapidly attracting to the fixed wire within a finite time. In this case, the pull-in phenomenon occurs.

In this section, based on the mathematical analysis presented in the previous section, we systematically investigate the dynamic behavior of the MEMS actuator from two distinct perspectives: (1) the influence of the mass's initial position on the system response, and (2) the combined effects of driving current parameters and spring stiffness coefficients under zero initial position conditions. This comparative analysis provides a comprehensive understanding of the system's sensitivity to initial conditions and its dependence on key control parameters, offering valuable insights for optimizing the performance of MEMS actuators in real-world applications.

3.1. Dynamical behaviors and critical thresholds

Recall from Theorem 2.2 in the previous section that the solutions to equation (2.1), subject to the initial conditions $x(0) = x_0$ and $x'(0) = 0$, may exhibit one of the following behaviors: finite-time blow-up, convergence to a constant as $t \to \infty$, periodic oscillations, or persistent consistency. In the context of MEMS actuators, these mathematical behaviors correspond to physical phenomena such as the occurrence of pull-in instability, the maintenance of an equilibrium state, or the emergence of periodic motion.

Theorem 3.1. *Consider the micro-electromechanical system governed by equation* (2.1)*, actuated at the initial state* $x(0) = x_0$ *with zero initial speed (i.e.,* $x'(0) = 0$*), where* $x_0 < 1$*. Let* x_1 *denote the unique zero of the cubic equation* $4kx^3 - 3kx^2 + 2x - 1 = 0$ *for* $k > 0$*. The system exhibits the following behaviors:*

(i) Pull-in instability occurs in the following cases:

- $I > \phi(x_1)$*;*
- $I = \phi(x_1)$ *and* $x_0 \neq x_1$*;*
- $0 < I < \phi(x_1)$ *and* $x_0 < x_c$ *or* $x_{e_2} < x_0 < 1$*.*

(ii) System maintains an equilibrium state under the following conditions:

- $I = \phi(x_1)$ *and* $x_0 = x_1$*;*
- $0 < I < \phi(x_1)$ *and* $x_0 = x_{e_1}$ *or* $x_0 = x_{e_2}$*.*

(iii) The movable wire exhibits periodic oscillations for $0 < I < \phi(x_1)$ *when* $x_0 \in (x_c, x_{e_1}) \cup (x_{e_1}, x_{e_2})$*, where* x_c *is determined by the condition* $h(x_c) = h(x_{e_2})$*. However, the movable wire tends to an equilibrium state when* $x_0 = x_c$*.*

Remark 3.1. We remark that the initial position $x_0 = 0$ corresponds to the spring being in its undeformed state, while $x_0 < 0$ indicates that the spring is compressed, and $x_0 > 0$ signifies that the spring is stretched. Furthermore, the relationship between I and $\phi(x_1)$ reflects the interplay between the driving currents in the wires and the stiffness of the spring, providing critical insights into the system's dynamic behavior. It is more convenient to denote the critical bifurcation value $\phi(x_1)$ by $I_c(k)$ since x_1 is uniquely determined by the stiffness coefficient of the spring k.

We can see from Theorem 3.1 that x_c is a critical value for the case when $0 < I < \phi(x_1)$. For a given I, x_c is determined by $h(x_c) = h(x_{e_2})$, that is,

$$\frac{1}{4}k(x_{e_2}^4 - x_c^4) + \frac{1}{2}(x_{e_2}^2 - x_c^2) + I \ln \frac{1 - x_{e_2}}{1 - x_c} = 0, \tag{3.1}$$

with $x_c < x_{e_1}$. Therefore, x_c is inherently defined by I and k, as x_{e_2} itself is a function of I and k.

Based on practical considerations, most MEMS devices start from a zero state. Therefore, we here consider the case with zero initial conditions $x(0) = x'(0) = 0$. It follows from Theorem 3.1 that if the movable wire tends to an equilibrium state x_{e_2} when $x_c = 0$, then there exists a critical value I_0 for I such that

$$\frac{1}{4}kx_{e_2}^4 + \frac{1}{2}x_{e_2}^2 + I_0 \ln(1 - x_{e_2}) = 0.$$

Recall that x_{e_2} is a zero of equation $x(x-1)(kx^2+1) + I_0 = 0$. Therefore, the critical value I_0 for I can be expressed as

$$I_0 = x_{e_2}(1 - x_{e_2})(kx_{e_2}^2 + 1), \tag{3.2}$$

where $0 < x_{e_2} < 1$ is determined implicitly by equation

$$\frac{1}{4}kx^3 + \frac{1}{2}x + (1-x)(kx^2+1)\ln(1-x) = 0. \tag{3.3}$$

Theorem 3.2. *In the context of a parallel-wire magneto-electro MEMS actuator, set the fixed wire at $x = 1$, and the movable wire initially at $x = 0$ with zero initial velocity. There is a critical current I_0 determined by equations* (3.2) *and* (3.3) *such that*

(1) Pull-in occurs when $I > I_0$;

(2) The movable wire tends to an unstable equilibrium state when $I = I_0$;

(3) Periodic movement emerges when $0 < I < I_0$.

As demonstrated in the preceding theorem, while the critical threshold I_0 for parameter I can be implicitly defined by equations (3.2) and (3.3), the explicit determination of I_0 remains analytically challenging due to the inherent nonlinearity of these equations. This computational complexity is similarly manifested in the determination of the critical value x_1, which is uniquely specified by the cubic equation $4kx^3 - 3kx^2 + 2x - 1 = 0$. Although x_1 admits an explicit representation of the form

$$\begin{aligned} x_1 =& \frac{k^{-\frac{1}{3}}}{12}\left(12\sqrt{3}\sqrt{\frac{27k^2-9k+32}{k}} + 27k + 108\right)^{\frac{1}{3}} \\ &+ \left(\frac{3k}{4} - 2\right)k^{-\frac{2}{3}}\left(12\sqrt{3}\sqrt{\frac{27k^2-9k+32}{k}} + 27k + 108\right)^{-\frac{1}{3}} + \frac{1}{4}, \end{aligned} \tag{3.4}$$

the practical implementation of this closed-form solution is nearly impossible, particularly when evaluating the bifurcation value $I_c(k) = \phi(x_1)$. The complexity caused by the intricate algebraic structure of the solution necessitates the use of numerical methods to approximate and analyze these critical values.

3.2. Numerical detection of the thresholds

We now proceed with numerical computations to validate our analytical findings. Substitution of $k = 0.1$ into the exact formula (3.4) or directly into the cubic equation (3.3) both lead to $x_1 = \frac{1}{12}\left(1107 + 12\sqrt{94110}\right)^{\frac{1}{3}} - \frac{77}{4}\left(1107 + 12\sqrt{94110}\right)^{-\frac{1}{3}} +$

$\frac{1}{4} \approx 0.5124762630$. With the help of Maple, we get $I_c(1) = \phi(x_1) = 0.2564060531$, which is the bifurcation value of I for the MEMS with $k = 0.1$. To further explore the system's behavior, we select three distinct values of I: $I = 0.5$, $I = I_c(0.1) = 0.2564060531$ and $I = 0.2$, to plot the phase portraits of the system (2.2) shown in Fig. 2.

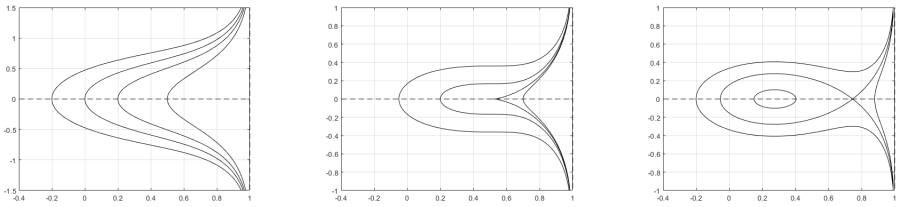

(a) $I = 0.5$ (b) $I = I_c(1) = 0.2564060531$ (c) $I = 0.2$

Figure 2. Phase portraits of system (2.2) with $k = 0.1$

To examine the solutions for the case when $I = 0.2$ which is less than $I_c(0.1)$, we need to calculate the two equilibrium states and the critical initial position x_c. The numerical solutions yield the roots $x_{e_1} = 0.2731064166$ and $x_{e_2} = 0.7460592208$. Additionally, by solving equation $H(x_{e_2}, 0) = H(x_c, 0)$, we determine the critical initial position $x_c = -0.05375314680$. To verify the consistency of our analytical results, we plot the system's trajectories using the following initial values: $x_0 = -0.2$, x_c, 0.1, 0.849, x_{e_1} and x_{e_2}. The resulting trajectories and solutions, as depicted in Fig. 3, demonstrate a strong agreement between the numerical outcomes and the analytical predictions. This consistency underscores the reliability of our theoretical framework and numerical approach.

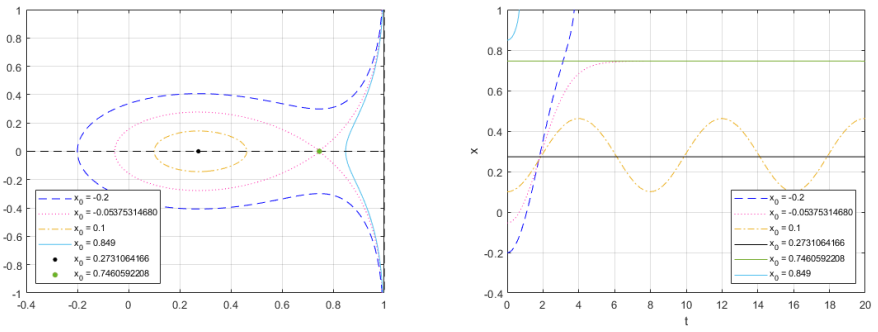

(a) Trajectories for distinct values of x_0 (b) Solution curves for distinct values of x_0

Figure 3. Phase portrait and corresponding solution curves for equation (2.1) with $k = 0.1$ and $I = 0.2$.

To observe the dynamical behavior and detect the thresholds for the MEMS actuated at $x = 0$ with zero initial velocity, we solve (3.3) with $k = 0.1$ numerically to have $x_{e_2} = 0.7270724212$, and thus we have $I_0 = 0.2089282351$ from equation (3.2). To verify the consistency of our analytical results in Theorem 3.2, we plot the system's trajectories with zero initial values $x(0) = x'(0) = 0$ and using the following values for I: 0.1, 0.2089282351, and 0.4. The resulting trajectories and

solutions are depicted in Fig. 4, which demonstrate a strong agreement between the numerical outcomes and the analytical predictions.

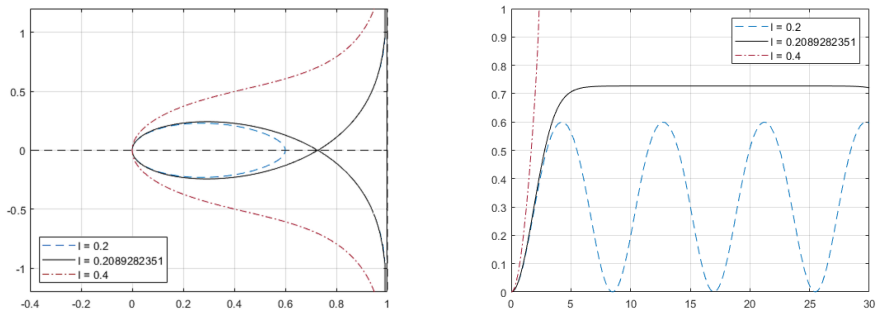

(a) Trajectories for distinct values of I (b) Solution curves for distinct values of I

Figure 4. Trajectories and corresponding solution curves for equation (2.1) with $k = 0.1$ and $x_0 = 0$.

The case that $k = 1$ has been considered in [19] and the threshold obtained there is $I_c = 0.2777$. To compare the results, we make the same setting that $k = 1$, and get $x_{e_2} = 0.7999287163$ from equation (3.3) and $I_c = 0.2624518820$ from equation (3.2). To check the correctness of these two results, we plot the trajectories for system (2.2) with $I = 0.2777$ and $I = 0.2624518820$ are plotted numerically (see Fig. 5). It shows that the threshold founded in [19] is inaccurate.

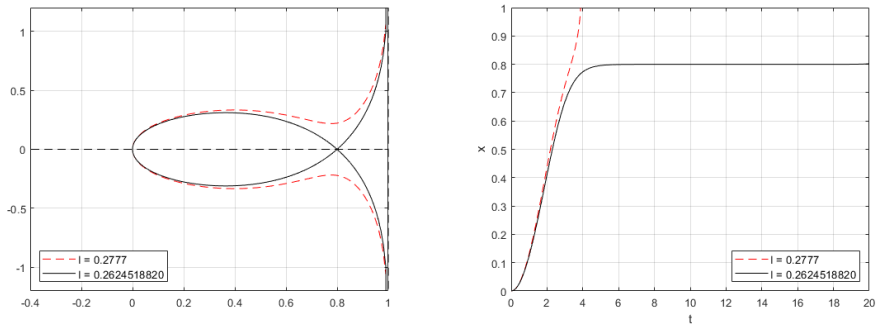

(a) Trajectories comparison (b) Solution curves comparison

Figure 5. Validation of threshold analysis: numerical simulation results compared with Ref. [19] for $k = 1$.

4. Conclusion

In this work, we have investigated the dynamic behavior and pull-in instability of a magneto-electro MEMS actuator with a nonlinear hardening spring. By deriving the governing equation based on Newton's Second Law and incorporating the nonlinear restoring force, a theoretical framework to analyze the system's critical

bifurcation value and the stability conditions is established. Using qualitative and bifurcation theories, we characterize the phase portraits and identify the conditions under which pull-in instability occurs. The analytical results are validated through numerical simulations, which demonstrate excellent agreement with the theoretically predicted threshold. The results highlight the significant role of nonlinear stiffness and magnetic forces in determining the system's dynamic response and stability. This study rectifies certain inaccuracies in previous results while significantly enhancing the fundamental understanding of pull-in instability mechanisms. The findings provide valuable insights for optimizing both the design and control of MEMS devices incorporating nonlinear hardening springs.

Acknowledgements

We sincerely thank the anonymous reviewers for their insightful feedback and constructive suggestions, which have greatly improved the quality of this paper.

References

[1] S. D. Senturia, *Microsystem Design*, Springer, 2001.

[2] N. Maluf and K. Williams, *Introduction to Microelectromechanical Systems Engineering*, 2nd ed., Artech House, 2004.

[3] Y. Wang and Z. Li, *MEMS for Automotive and Aerospace Applications*, Springer, 2012.

[4] S. H. Kim and J. Lee, *MEMS for Consumer Electronics*, IEEE Press, 2017.

[5] A. H. Nayfeh and M. I. Younis, *Nonlinear Dynamics of MEMS and NEMS*, Wiley, 2008.

[6] W. M. Zhang and G. Meng, *Nonlinear Dynamics of MEMS Resonators*, Springer, 2010.

[7] M. I. Younis, *MEMS Linear and Nonlinear Statics and Dynamics*, Springer, 2011.

[8] J. F. Rhoads and S. W. Shaw, *Nonlinear Dynamics of Microelectromechanical Systems*, Cambridge University Press, 2010.

[9] P. M. Osterberg and S. D. Senturia, *M-TEST: A Test Chip for MEMS Material Property Measurement*, Journal of Microelectromechanical Systems, 1997, 6(2), 107–118.

[10] E. S. Hung and S. D. Senturia, *Extending the Travel Range of Analog-Tuned Electrostatic Actuators*, Journal of Microelectromechanical Systems, 2002, 11(1), 1–10.

[11] A. H. Nayfeh, M. I. Younis, and E. M. Abdel-Rahman, *Dynamic Pull-In Phenomenon in MEMS Resonators*, Nonlinear Dynamics, 2007, 48(1–2), 153–163.

[12] W. M. Zhang, H. Yan, and Z. K. Peng et al., *Electrostatic Pull-In Instability in MEMS/NEMS: A Review*, Sensors and Actuators A: Physical, 2014, 214, 187–218.

[13] D. J. Griffiths, *Introduction to Electrodynamics*. 4th ed., Cambridge University Press, 2017.

[14] J. H. He, D. Nurakhmetov, and P. Skrzypacz et al., *Dynamic Pull-In for Micro-Electromechanical Device with a Current-Carrying Conductor*, Journal of Low Frequency Noise, Vibration and Active Control, 2019, 0(0), 1–8.

[15] P. Skrzypacz, G. Ellis, and J. H. He, Dynamic Pull-In and Oscillations of Current-Carrying Filaments in Magnetic Micro-Electro-Mechanical System, Communications in Nonlinear Science and Numerical Simulation, 2022, 109, 106350.

[16] C. Y. Wang, P. A. He, and L. J. Zhang et al., Research on Dynamic Pull-In Threshold of Micro-Electro-Mechanical Systems with Current-Carrying Conductors, Journal of Zhejiang Sci-Tech University, 2020, 43(3), 389–393.

[17] X. S. Liu, L. J. Zhang, and M. J. Zhang, *Studies on Pull-In Instability of an Electrostatic MEMS Actuator: Dynamical System Approach*, Journal of Applied Analysis and Computation, 2022, 12(2), 850–861.

[18] Q. G. Yuan, Z. B. Cheng, and X. P. Li, *Dynamics of Periodic Solution to an Electrostatic Micro-Electro-Mechanical System*, Communications in Nonlinear Science and Numerical Simulation, 2023, 116, 106828.

[19] Q. Yang, *A Mathematical Control for the Pseudo-Pull-In Stability Arising in a Micro-Electromechanical System*, Journal of Low Frequency Noise, Vibration and Active Control, 2022, 0(0), 1–8.

[20] J.B. Li, G.R. Chen, *More on bifurcations and dynamics of traveling wave solutions for a higher-order shallow water wave equation*, International Journal of Bifurcation and Chaos, 2019, 29(01), 1950014.

[21] L.J. Zhang, J.D. Wang, E. Shchepakina, V. Sobolev, *New solitary waves in a convecting fluid*, Chaos Soliton Fractals. 2024, 183, 114953.

[22] L.J. Zhang, M.A. Han, M.J. Zhang, C.M. Khalique, *A new type of solitary wave solution of the mKdV equation under singular perturbations,* International Journal of Bifurcation and Chaos, 2020, 30(11), 2050162.

[23] L. Perko, *Differential equations and dynamical systems*, Springer Science and Business Media, 2013.